POLYOXOMETALATES RESEARCH ARTICLE

Tricine-supported polyoxo(alkoxo)lanthanide cluster $\{Ln_{15}\}$ (Ln = Eu, Gd, Tb) with magnetic refrigerant and fluorescent properties

Peng-Fei Sun, Xiao-Nan Zhang, Cai-Hong Fan, Wei-Peng Chen ✉, and Yan-Zhen Zheng ✉

Frontier Institute of Science and Technology, State Key Laboratory of Mechanical Behavior for Materials, MOE Key Laboratory for Nonequilibrium Synthesis of Condensed Matter, Xi'an Key Laboratory of Sustainable Energy and Materials Chemistry, School of Chemistry, Xi'an Jiaotong University, Xi'an 710054, China

Cite This: *Polyoxometalates*, **2023**, *2*, 9140026 Read Online

ABSTRACT: A family of polyoxo(alkoxo)lanthanide cluster $\{Ln_{15}\}$ (Ln = Eu (**1**), Gd (**2**), Tb (**3**)) was successfully isolated via a simple hydrolysis reaction of lanthanide metal ions in the presence of tricine ligands. X-ray diffraction analyses revealed that $\{Ln_{15}\}$ displayed a wheel-like structure with a μ_5-chloride anion as a template. Interestingly, each analog showed distinctive functions based on the different Ln(III) ions. Complexes **1** and **3** in the solid state emitted the characteristic fluorescence of Eu(III) or Tb(III). The fluorescence lifetimes of the $^5D_0$ excited state for **1** and the $^5D_4$ excited state for **3** were tested, and the values were 890 and 250 μs, respectively. Meanwhile, gadolinium analog **2** exhibited a magneto-caloric effect at ultralow temperatures with a maximum $-\Delta S_m$ value of 29.9 $J \cdot kg^{-1} \cdot K^{-1}$ at 3 K and 7 T.

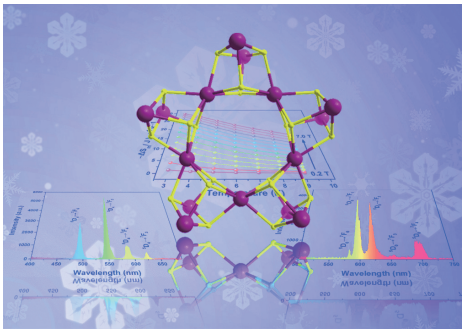

KEYWORDS: polymetallic complexes, lanthanide elements, luminescence, magnetic refrigeration, magnetic exchange

1 Introduction

Polymetallic complexes, such as polyoxometalates, coinage metal aggregations, transition/transition-rare earth metal clusters, and so on, are of great interest not only for their appealing molecular structures but also for their versatile applications in various fields [1–10]. Among these, lanthanide polynuclear compounds have drawn unprecedented attention because of their interesting magnetic and luminescence behaviors, which may be attributed to the different f-electron configurations of lanthanide ions [11–17]. For instance, Gd(III) plays a crucial role in the exploitation of magnetic refrigerants because of its large spin ground state and low anisotropy [11, 12]. Eu(III), Tb(III), Er(III), and Yb(III) ions are typically preferred for constructing luminescent materials [15–17]. Meanwhile, the Dy(III) ion is mainly utilized for the exploitation of single-molecular magnets because of its magnetic anisotropy arising from a large, unquenched orbital angular momentum [13, 14]. Until now, many lanthanide polynuclear aggregations with different properties have been successfully isolated, such as $\{Ln_{20}\}$, $\{Ln_{24}\}$, $\{Ln_{36}\}$ $\{Ln_{38}\}$, $\{Ln_{42}\}$, $\{Ln_{48}\}$, $\{Ln_{60}\}$, $\{Ln_{72}\}$, $\{Ln_{104}\}$, and $\{Ln_{140}\}$ [18–26]. Nevertheless, because of the high coordination numbers and the diverse coordination geometries for 4f metal ions, the synthesis of lanthanide clusters is still a challenge [27–29].

Previous findings revealed that controlling the hydrolysis of lanthanide metal ions in the presence of appropriate organic ligands is a powerful strategy for obtaining such species [27–29]. One kind of the most widely used ligands is the N, O-ligand, such as oximes, Schiff bases, pyridoxol derivatives, hydramines, imino-diacetic acid, and so on [28]. Many lanthanide clusters have been prepared based on these ligands, including a few examples containing more than 15 metal centers [27–29]. However, lanthanide clusters based on the tricine ligand *n*-[2-droxy-1,1-bis(hydroxyl-methyl)ethyl]-glycin ($(HOCH_2)_3CNHCH_2CO_2H$, H_4L) have not yet been reported.

Tricine containing multiple O or OH arms and N-donors (Scheme 1), can exist in various forms depending on the basicity of the reaction solvent, such as singly, doubly, or triply protonated species [30]. The flexible OH arms of tricine ligands can not only accommodate a large range of ionic radii of metals but also form five- or six-membered rings with the metal ions just as amino polyalcohols, Schiff bases, and pyridoxol derivative can, which is beneficial for stabilizing the structures of such complexes. In addition, tricine's good solubility in various solvents, such as

Received: November 26, 2022; **Revised:** January 1, 2023
Accepted: February 13, 2023

✉Address correspondence to Wei-Peng Chen, sxchenweipeng@163.com; Yan-Zhen Zheng, zheng.yanzhen@xjtu.edu.cn

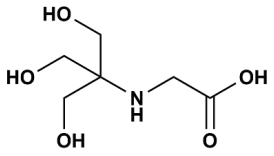

Scheme 1 Tricine (H_4L).

alcohol, and acetonitrile, benefits the construction of lanthanide clusters. Yet surprisingly, only a handful of tricine-based mononuclear coordination complexes have been reported [31–33]. Herein, we report a family of polyoxo(alkoxo)lanthanide clusters $\{Ln_{15}\}$ prepared from the reaction of tricine ligands.

Through a simple hydrolysis reaction, three isostructural lanthanide nanoclusters, $[Eu_{15}(\mu_3\text{-}OH)_{20}(\mu_5\text{-}Cl)(H_3L)_8(H_2L)_2(H_2O)_{10}](Cl)_3\cdot(NO_3)_9\cdot20H_2O\cdot4CH_3OH$ (**1**), $[Gd_{15}(\mu_3\text{-}OH)_{20}(\mu_5\text{-}Cl)(H_3L)_8(H_2L)_2(H_2O)_{10}](Cl)_3\cdot(NO_3)_9\cdot22H_2O\cdot3CH_3OH$ (**2**), and $[Tb_{15}(\mu_3\text{-}OH)_{20}(\mu_5\text{-}Cl)(H_3L)_8(H_2L)_2(H_2O)_{10}](Cl)_4\cdot(NO_3)_8\cdot22H_2O\cdot5CH_3OH$ (**3**), were successfully synthesized. X-ray diffraction analyses revealed that $\{Ln_{15}\}$ displays a wheel-shaped structure with a μ_5-chloride anion as a template. Because of the presence of different lanthanide metal ions in these analogs, each compound showed distinctive properties. Complexes **1** and **3** in the solid state emitted the characteristic fluorescence of Eu(III) or Tb(III). The fluorescence lifetimes of the $^5D_0$ excited state for **1** and the $^5D_4$ excited state for **3** were tested, and the values were 890 and 250 μs, respectively. Meanwhile, gadolinium analog **2** exhibited a magneto-caloric effect at ultralow temperatures with a maximum $-\Delta S_m$ value of 29.9 $J\cdot kg^{-1}\cdot K^{-1}$ at 3 K and 7 T.

2 Experimental

2.1 Materials and methods

All reagents and solvents for the syntheses were purchased from commercial sources and used as received. C, H, and O element analyses were conducted on a Flash 2000 elemental analyzer. The samples' infrared (IR) spectra were collected on a Bruker Alpha FT-IR spectrophotometer using KBr pellets in the range of 4000–600 cm^{-1}. Thermogravimetric (TG) spectra were measured using a TGA-2 (METTLER TOLEDO) thermogravimetric analyzer. Powder X-ray diffraction (PXRD) data of the samples were collected using a D8 ADVANCE Bruker X-Ray diffractometer (Cu Kα, λ = 1.54184 Å) at room temperature. The fluorescence spectra were recorded using a Hitachi F-4600 fluorescence spectrometer. Magnetic susceptibility measurements were performed on a powder sample fixed with eicosane on a Quantum Design MPMS-XL7 SQUID magnetometer.

2.2 Synthesis of $\{Ln_{15}\}$ (Ln = Eu (1), Gd (2), Tb (3))

Synthesis of $[Eu_{15}(\mu_3\text{-}OH)_{20}(\mu_5\text{-}Cl)(C_6H_{12}NO_5)_8(C_6H_{11}NO_5)_2(H_2O)_{10}](Cl)_3\cdot(NO_3)_9\cdot20H_2O\cdot4CH_3OH$ (1). *n*-[2-Hydroxy-1,1-bis(hydroxymethyl)ethyl]-glycine (0.36 g, 2.0 mmol), $Eu(NO_3)_3\cdot6H_2O$ (1.34 g, 3.0 mmol), and KCl (0.1 g, 0.13 mmol) were dissolved in a mixed solvent of CH_3OH/H_2O (10 mL, v/v = 1:1) under stirring. Triethylamine (0.56 mL, 4.0 mmol) was added drop by drop into the above clear solution. The colorless solution was filtered and left undisturbed for 3 days. Colorless crystals were isolated by filtration and washed with ethanol (yield: ~ 31.2% based on Eu). Elemental analysis calculated (%) for $C_{64}H_{214}N_{19}Cl_4Eu_{15}O_{131}$: C 13.3, H 3.7, N 4.6. Found (%): C 13.1, H 3.5, N 4.40. IR (KBr disk, see Fig. S1 in the Electronic Supplementary Material): σ = 3368(w), 3268(w), 3205(w), 1582(s), 1405(s), 1310(s), 1043(w), 1006(s), 658(w), 617(s), 550(w), 503(w).

Synthesis of $[Gd_{15}(\mu_3\text{-}OH)_{20}(\mu_5\text{-}Cl)(C_6H_{12}NO_5)_8(C_6H_{11}NO_5)_2(H_2O)_{10}](Cl)_3\cdot(NO_3)_9\cdot22H_2O\cdot3CH_3OH$ (2). Complex **2** was obtained following the same procedure using $Gd(NO_3)_3\cdot6H_2O$ instead of $Eu(NO_3)_3\cdot6H_2O$. The yield was ~ 29.2% based on Gd. Elemental analysis calculated (%) for $C_{63}H_{214}N_{19}Cl_4Gd_{15}O_{132}$: C 13.0, H 3.7, N 4.5. Found (%): C 13.1, H 3.5, N 4.40. Infrared (KBr disk, Fig. S1 in the ESM): σ = 3378(w), 3266(w), 3201(w), 1585(s), 1408(s), 1315(s), 1040(w), 1003(s), 668(w), 621(s), 551(w), 504(w).

Synthesis of $[Tb_{15}(\mu_3\text{-}OH)_{20}(\mu_5\text{-}Cl)(C_6H_{12}NO_5)_8(C_6H_{11}NO_5)_2(H_2O)_{10}](Cl)_3\cdot(NO_3)_9\cdot22H_2O\cdot20CH_3OH$ (3). Complex **3** was obtained following the same procedure using $Tb(NO_3)_3\cdot6H_2O$ instead of $Eu(NO_3)_3\cdot6H_2O$. The yield was ~ 35.4% based on Tb. Elemental analysis calculated (%) for $C_{65}H_{222}N_{19}Cl_4Tb_{15}O_{134}$: C 13.2, H 3.8, N 4.5. Found (%): C 13.1, H 3.5, N 4.42. IR (KBr disk, Fig. S1 in the ESM): σ = 3377(w), 3268(w), 3200(w), 1589(s), 1405(s), 1310(s), 1048(w), 1007(s), 703(w), 622(s), 549(w), 517(w).

2.3 X-ray crystallography

Because of the weak diffracted intensity of the single crystals for **1** and **3**, only the single-crystal X-ray diffraction data of **2** were collected on a Bruker Apex II diffractometer with Mo Kα radiation (λ = 0.71073 Å) at 150 K. The structure was solved using direct methods, and all non-H atoms were subjected to anisotropic refinement through full-matrix least-squares refinement on F^2 using the Olex2 program. There were three disordered methanol and 22 water molecules per formula unit, which were removed by SQUEEZE in the refinement but accurately confirmed by elemental and TG analyses (Fig. S2 in the ESM). The refinement parameters and crystallographic data for complex **2** are shown in Table 1. CCDC 2191867 contains supplementary crystallographic data. These data can be obtained free of charge via www.ccdc.cam.ac.uk/data_request/cif. The crystal cell parameters and PXRD spectra for complexes **1** and **3** are shown in Table S1 and Fig. S3 in the ESM, respectively.

3 Results and discussion

Single crystal X-ray diffraction analyses revealed that complexes **1–3** are isostructural, differing only in the number of guest molecules in the lattice. Thus, only the detailed description of **2** is given below. Compound **2** crystallized in the monoclinic space group *C*2/*c* with *Z* = 4. As represented in Fig. 1, the wheel-like $\{Gd_{15}(\mu_3\text{-}OH)_{20}\}$ core consisted of five $\{Gd_4(\mu_3\text{-}OH)_4\}$ cubane-like subunits by sharing five Gd(III) corners around a μ_5-chloride anion. Ten deprotonated tricine ligands adopting 3.21111 bridging modes (Harris notation) provided the key linkages between the adjacent $\{Gd_4(\mu_3\text{-}OH)_4\}$ building blocks [34–36]. The deprotonated forms of the tricine ligand are shown in Fig. S4 in the ESM [35]. All the Gd(III) ions in the $\{Gd_{15}\}$ core were nona-coordinated. For the ten peripheral ones, the coordination spheres featured one coordinated water, three μ_3-OH^- groups, one N atom, and four O atoms from the tricine ligand, respectively. Meanwhile, the five inner shared Gd(III) ions were each coordinated by one chloride ion, six μ_3-OH^- groups, and two O atoms from the carboxyl groups of two tricine ligands. The Gd···Gd separations within the $Gd_4(\mu_3\text{-}OH)_4$ subunits were 3.65–4.05 Å, and the Gd–O, Gd–N, and Gd–Cl bond lengths ranged from 2.34 to 2.57, 2.57 to 2.60 and 3.21 to 3.26 Å,

Table 1 Crystal data and structure refinements for complex $\{Gd_{15}\}$ **2**[a]

Empirical formula	$C_{63}H_{214}N_{19}Cl_4Gd_{15}O_{132}$
Formula weight	5851.0
Crystal system	Monoclinic
Space group	$C2/c$
a (Å)	40.213(6)
b (Å)	21.621(3)
c (Å)	27.359(4)
α (°)	90
β (°)	131.3520(10)
γ (°)	90
Volume (Å^3)	17,855(5)
Z	4
F(000)	1.787
Crystal size (mm)	0.09 × 0.21 × 0.23
2θ range (°)	2.698 to 50
Reflections collected	84,340
Independent reflections	15,708 (R_{int} = 0.0650, R_{sigma} = 0.0485)
Data/restraints/parameters	15,708/520/893
Goodness-of-fit on F^2	1.082
Final R indexes ($I \geq 2\sigma(I)$)	R_1 = 0.0362, wR_2 = 0.0904
Final R indexes (all data)	R_1 = 0.0560, wR_2 = 0.1006
Largest diff. peak/hole (e/Å^3)	1.55/−1.10

[a] $R_1 = \Sigma||F_o| - |F_c||/\Sigma|F_o|$, $wR_2 = [\Sigma w(F_o^2 - F_{c2})_2/\Sigma w(F_{o2})_2]_{1/2}$.

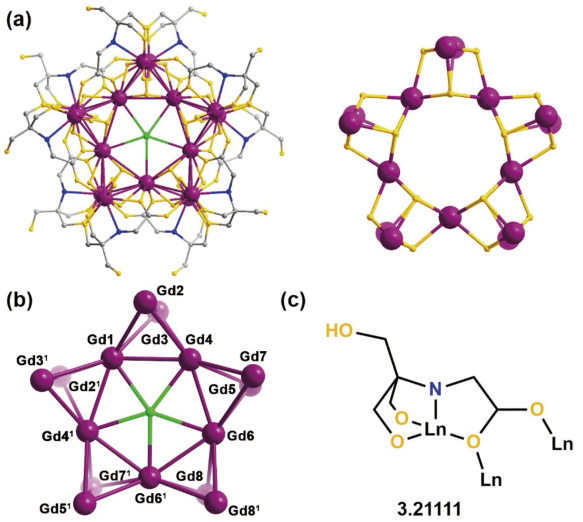

Figure 1 Ball-and-stick views of **2** with H atoms removed for clarity. (b) Arrangement of metal centers in the $[Gd_{15}]$ core. Symmetry codes: 1−x, y, 1.5−z. (c) Coordination mode of the tricine ligand. Color code: Gd, purple; Cl, green; O, yellow; N, blue; C, gray.

respectively, close to the distances reported for other polymetallic lanthanide clusters [36–38]. The selected bond lengths (Å) for **2** are shown in Table S2 in the ESM. Continuous shape measure analyses using the SHAPE program were performed to determine the degree of deviation from the ideal polyhedron to gain further insight into the coordination geometry of metal centers in complex **2**. The coordination geometries and the SHAPE calculation results are shown in Table S3 in the ESM.

Because of the unique and intriguing optical properties of Eu(III) and Tb(III) ions, the solid-state photoluminescence spectra for **1** and **3** were recorded at room temperature to explore their luminescence behaviors (Fig. 2). As shown in Fig. 2(a), when monitoring the Eu(III) emission at 594 nm, the excitation spectrum of **1** showed a band maximum at around 395 nm, corresponding to the $^7F_0 \rightarrow {}^5L_6$ transition of the Eu(III) ion. Under 395-nm excitation, **1** exhibited the characteristic transitions of the Eu(III) ion at 582 ($^5D_0 \rightarrow {}^7F_0$), 594 ($^5D_0 \rightarrow {}^7F_1$), 619 ($^5D_0 \rightarrow {}^7F_2$), 654 ($^5D_0 \rightarrow {}^7F_3$), and 698 ($^5D_0 \rightarrow {}^7F_4$) nm, respectively, corresponding to 4f–4f transitions from the resonating level $^5D_0$ to the ground state multiplet ^7F_J (J = 0, 1, 2, 3, and 4) of the Eu(III) ion [39]. For compound **3**, four characteristic peaks of the Tb(III) ion were observed at 491 ($^5D_4 \rightarrow {}^7F_6$), 548 ($^5D_4 \rightarrow {}^7F_5$), 587 ($^5D_4 \rightarrow {}^7F_4$), and 623 ($^5D_4 \rightarrow {}^7F_3$) nm, respectively. Then, the decay lifetimes of complexes **1** and **3** were investigated to better understand their luminescence properties. As shown in Fig. 3(a), the decay curves for **1** and **3** were found to be well fitted with the exponential equation $I_t = I_0 + Ae^{-t/\tau}$ (I_0, the maximum luminescence intensity; I_t, the luminescence intensity at t; A, the constant; τ, the decay lifetime) [40, 41] and revealed the lifetimes of 890 and 250 μs, respectively. Meanwhile, the quantum yields of 11.18% for **1** and 22.36% for **3** were also measured.

The images of polycrystalline samples for **1** and **3** under ultraviolet light are shown in Fig. 3(b). Complexes **1** and **3** displayed red and green emissions, respectively, which clearly show the effect of different lanthanide ions on luminescence properties. The Commission Internationale de L'Eclairage (CIE) chromaticity was also determined according to their corresponding photoluminescence spectra (Fig. 3(b)), and complexes **1** and **3**

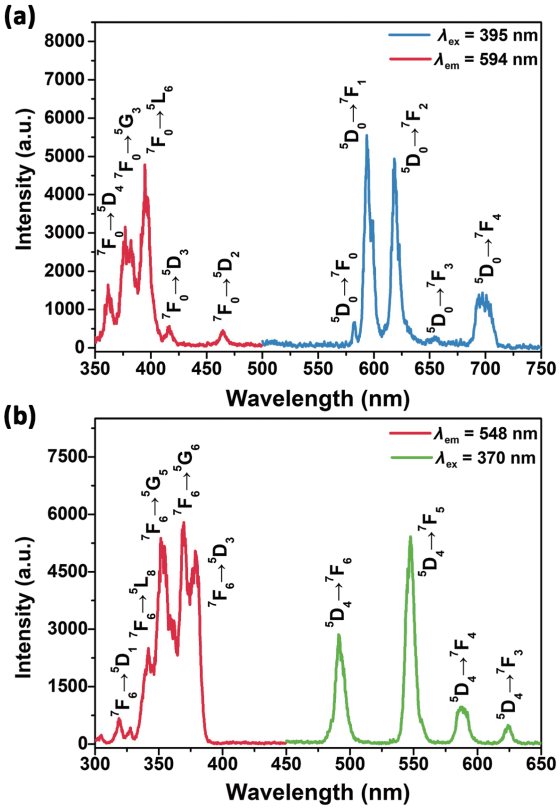

Figure 2 Excitation and emission spectra for complexes **1** (a) and **3** (b).

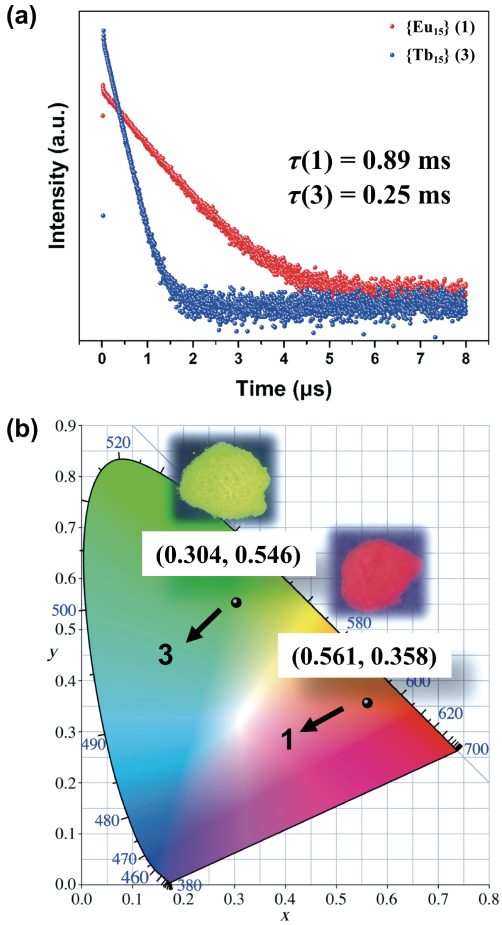

Figure 3 (a) Photoluminescence decay curves of **1** (λ_{ex} = 395 nm and λ_{em} = 594 nm) and **3** (λ_{ex} = 370 nm and λ_{em} = 548 nm). (b) CIE diagram for the emission spectra of **1** and **3**. Inset: fluorescent images for complexes **1** and **3** taken under ultraviolet light.

notably can emit red and green in the visible region with the chromaticity coordinates of (0.561, 0.358) and (0.304, 0.546), respectively. Because the color temperature varied from red to white to blue, only the color temperature of compound **1** must be calculated. The color temperature for **1** was calculated as 1457 K, which corresponded with the CIE chromaticity.

The direct-current susceptibility data of complex **2** were collected under an applied magnetic field of 1000 Oe between 2 and 300 K. As shown in Fig. 4(a), the $\chi_m T$ product of 113.44 cm³·K·mol⁻¹ at room temperature was slightly lower than the theoretical value of 118.1 cm³·K·mol⁻¹ for 15 uncorrelated Gd(III) ions (S = 7/2, g = 2). Upon cooling, the $\chi_m T$ value stayed practically constant at about 60 K and then sharply decreased to a minimum value of 73.2 cm³·K·mol⁻¹ at 2 K, indicating the presence of antiferromagnetic interactions between the Gd(III) centers. The χ_m^{-1} vs. T plot in the range of 50–300 K can be nicely fitted into the Curie–Weiss equation, producing the Curie constant C = 114.91 cm³·K·mol⁻¹ and the Weiss constant θ = −1.27 K (Fig. 4(a), inset), which further support the presence of weak antiferromagnetic interactions.

Magnetization measurements for **2** at low temperatures (2.0–10 K) were conducted in the 0- to 7-T field range (Fig. 4(b)). The M vs. H data displayed a steady increase in magnetization to reach 86.6 $N\mu_B$ at 2 K and 7 T without achieving saturation (where N is the Avogadro constant and μ_B is the Bohr magneton). This value is lower than the expected saturation value of 105 $N\mu_B$, which can be

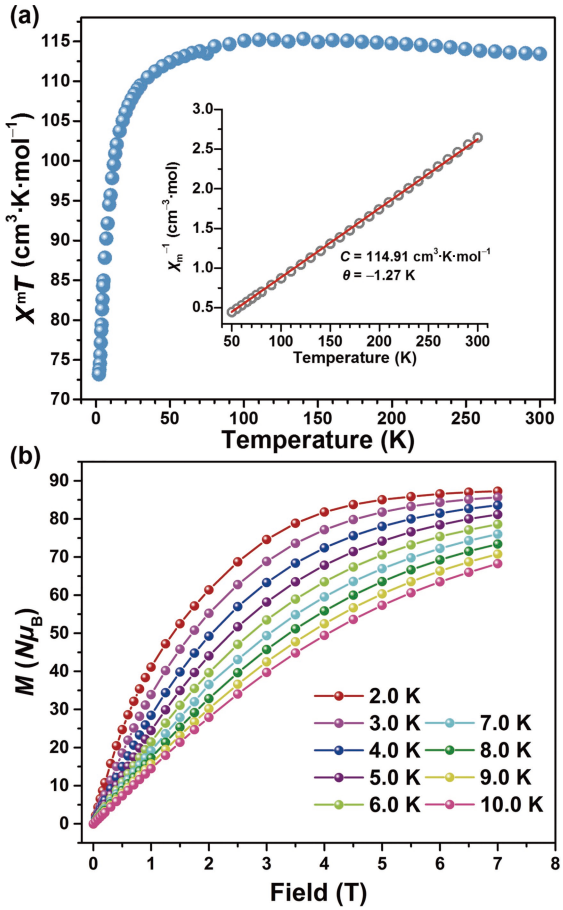

Figure 4 (a) Temperature dependence plots of $\chi_m T$ for **2**. Inset: plot of χ_m^{-1} vs. T for **2**. (b) Plots of field-dependent magnetization for **2**.

attributed to the presence of antiferromagnetic exchanges. Because complex **2** is a possible candidate for magnetic refrigeration materials, the magnetic entropy changes ΔS_m of this complex were evaluated by applying the Maxwell relation $-\Delta S(T)_{\Delta B} = \int[\partial M(T,B)/\partial T]_B dB$ based on the above magnetization data. The resulting maximum value at 3 K and 7 T for **2** is 29.9 J·kg⁻¹·K⁻¹ (Fig. 5), which is comparable with those of other reported polymetallic Gd clusters (Table S4 in the ESM). The maximum entropy change was calculated using the equation $-\Delta S_M = nR\ln(2S+1) = 31.2R$. The large discrepancy could be attributed to the antiferromagnetic exchanges among the Gd(III) centers.

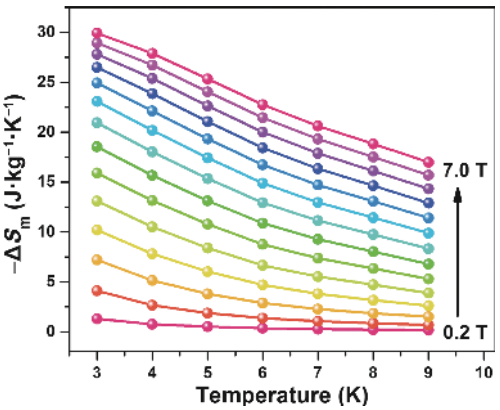

Figure 5 $-\Delta S_m$ values calculated from the magnetization data of **2**.

4 Conclusions

In summary, a series of wheel-like isostructural lanthanide clusters [Ln_{15}] (Ln = Eu (**1**), Gd (**2**), and Tb (**3**)) based on the tricine ligand was successfully synthesized via the hydrolysis reaction. Interestingly, each analog showed distinctive functions based on different Ln ions. Complexes **1** and **3** displayed red and green emissions, respectively, whereas gadolinium analog **2** exhibited potential application in magnetic cooling. Further work on tricine-based clusters is under investigation.

Electronic Supplementary Material: Supplementary material (the cif file, PXRD spectra, IR spectra, TG curves and other necessary tables) is available in the online version of this article at https://doi.org/10.26599/POM.2023.9140026.

Acknowledgements

This work was supported by the National Natural Science Foundation of China (No. 21971203), Special Support Plan of Shaanxi Province for Young Top-notch Talent, the Instrument Analysis Center of Xi'an Jiaotong University for assistance, and Fundamental Research Funds for Central Universities.

Declaration of competing interest

The authors have no competing interests to declare that are relevant to the content of this article.

Author contribution statement

The manuscript was written through contributions of all authors.

References

[1] Chen, L.; Chen, W. L.; Wang, X. L.; Li, Y. G.; Su, Z. M.; Wang, E. B. Polyoxometalates in dye-sensitized solar cells. *Chem. Soc. Rev.* **2019**, *48*, 260–284.

[2] Liu, J. X.; Zhang, X. B.; Li, Y. L.; Huang, S. L.; Yang, G. Y. Polyoxometalate functionalized architectures. *Coord. Chem. Rev.* **2020**, *414*, 213260.

[3] Patel, A.; Sadasivan, R. Modified Mn substituted POMs: Synthetic strategies, structural diversity to applications. *Prog. Mater. Sci.* **2021**, *118*, 100759.

[4] Moors, M.; Warneke, J.; López, X.; de Graaf, C.; Abel, B.; Monakhov, K. Y. Insights from adsorption and electron modification studies of polyoxometalates on surfaces for molecular memory applications. *Acc. Chem. Res.* **2021**, *54*, 3377–3389.

[5] Zhang, M. M.; Dong, X. Y.; Wang, Y. J.; Zang, S. Q.; Mak, T. C. W. Recent progress in functional atom-precise coinage metal clusters protected by alkynyl ligands. *Coord. Chem. Rev.* **2022**, *453*, 214315.

[6] Yin, B. Q.; Luo, Z. X. Coinage metal clusters: From superatom chemistry to genetic materials. *Coord. Chem. Rev.* **2021**, *429*, 213643.

[7] Yan, J. Z.; Teo, B. K.; Zheng, N. F. Surface chemistry of atomically precise coinage-metal nanoclusters: From structural control to surface reactivity and catalysis. *Acc. Chem. Res.* **2018**, *51*, 3084–3093.

[8] Huang, W. M.; Chen, W. M.; Bai, Q. X.; Zhang, Z.; Feng, M.; Zheng, Z. P. Anion-guided stepwise assembly of high-nuclearity lanthanide hydroxide clusters. *Angew. Chem., Int. Ed.* **2022**, *61*, e202205385.

[9] Huang, W. M.; Liu, Q. X.; Chen, W. M.; Feng, M.; Zheng, Z. P. Recent advances in the catalytic applications of lanthanide-oxo clusters. *Magnetochemistry* **2021**, *7*, 161.

[10] Zheng, X. Y.; Xie, J.; Kong, X. J.; Long, L. S.; Zheng, L. S. Recent advances in the assembly of high-nuclearity lanthanide clusters. *Coord. Chem. Rev.* **2019**, *378*, 222–236.

[11] Zheng, Y. Z.; Zhou, G. J.; Zheng, Z. P.; Winpenny, R. E. P. Molecule-based magnetic coolers. *Chem. Soc. Rev.* **2014**, *43*, 1462–1475.

[12] Liu, J. L.; Chen, Y. C.; Guo, F. S.; Tong, M. L. Recent advances in the design of magnetic molecules for use as cryogenic magnetic coolants. *Coord. Chem. Rev.* **2014**, *281*, 26–49.

[13] Liu, K.; Shi, W.; Cheng, P. Toward heterometallic single-molecule magnets: Synthetic strategy, structures and properties of 3d-4f discrete complexes. *Coord. Chem. Rev.* **2015**, *289–290*, 74–122.

[14] Marin, R.; Brunet, G.; Murugesu, M. Shining new light on multifunctional lanthanide single-molecule magnets. *Angew. Chem., Int. Ed.* **2021**, *60*, 1728–1746.

[15] Yang, X. P.; Wang, S. Q.; Wang, C. R.; Huang, S. M. ; Jones, R. A. Construction and luminescence properties of 4f and d-4f clusters with salen-type schiff base ligands. In *Recent Development in Clusters of Rare Earths and Actinides*: *Chemistry and Materials*; Zheng, Z. P., Ed.; Springer: Berlin Heidelberg, 2017; pp 155–187.

[16] Yang, X. P.; Schipper, D.; Jones, R. A.; Lytwak, L. A.; Holliday, B. J.; Huang, S. M. Anion-dependent self-assembly of near-infrared luminescent 24- and 32-metal Cd-Ln complexes with drum-like architectures. *J. Am. Chem. Soc.* **2013**, *135*, 8468–8471.

[17] Gálico, D. A.; Ovens, J. S.; Murugesu, M. NIR-to-NIR emission on a water-soluble {Er_6} and {Er_3Yb_3} nanosized molecular wheel. *Nanoscale* **2020**, *12*, 11435–11439.

[18] Gálico, D. A. ; Kitos, A. A. ; Ovens, J. S. ; Sigoli, F. A. ; Murugesu, M. Lanthanide-based molecular cluster-aggregates: Optical barcoding and white-light emission with nanosized {Ln_{20}} compounds. *Angew. Chem., Int. Ed.* **2021**, *60*, 6130–6136.

[19] Chang, L. X.; Xiong, G.; Wang, L.; Cheng, P.; Zhao, B. A 24-Gd nanocapsule with a large magnetocaloric effect. *Chem. Commun.* **2013**, *49*, 1055–1057.

[20] Wu, M. Y.; Jiang, F. L.; Kong, X. J.; Yuan, D. Q.; Long, L. S.; Al-Thabaiti, S. A.; Hong, M. C. Two polymeric 36-metal pure lanthanide nanosize clusters. *Chem. Sci.* **2013**, *4*, 3104–3109.

[21] Guo, F. S.; Chen, Y. C.; Mao, L. L.; Lin, W. Q.; Leng, J. D.; Tarasenko, R.; Orendáč, M.; Prokleška, J.; Sechovský, V.; Tong, M. L. Anion-templated assembly and magnetocaloric properties of a nanoscale {Gd_{38}} cage versus a {Gd_{48}} barrel. *Chem.—Eur. J.* **2013**, *19*, 14876–14885.

[22] Che, Z. W.; Chen, J. T.; Wang, T. T.; Yan, H.; Zhou, T. D.; Guo, R.; Sun, W. B. Wheel-like Gd_{42} polynuclear complexes with significant magnetocaloric effect. *CrystEngComm* **2022**, *24*, 3363–3368.

[23] Dong, J.; Cui, P.; Shi, P. F.; Cheng, P.; Zhao, B. Ultrastrong alkali-resisting lanthanide-zeolites assembled by [Ln_{60}] nanocages. *J. Am. Chem. Soc.* **2015**, *137*, 15988–15991.

[24] Qin, L.; Yu, Y. Z.; Liao, P. Q.; Xue, W.; Zheng, Z. P.; Chen, X. M.; Zheng, Y. Z. A "molecular water pipe": A giant tubular cluster {Dy_{72}} exhibits fast proton transport and slow magnetic relaxation. *Adv. Mater.* **2016**, *28*, 10772–10779.

[25] Peng, J. B.; Kong, X. J.; Zhang, Q. C.; Orendáč, M.; Prokleška, J.; Ren, Y. P.; Long, L. S.; Zheng, Z. P.; Zheng, L. S. Beauty, symmetry, and magnetocaloric effect-four-shell keplerates with 104 lanthanide atoms. *J. Am. Chem. Soc.* **2014**, *136*, 17938–17941.

[26] Zheng, X. Y.; Jiang, Y. H.; Zhuang, G. L.; Liu, D. P.; Liao, H. G.; Kong, X. J.; Long, L. S.; Zheng, L. S. A gigantic molecular wheel of {Gd_{140}}: A new member of the molecular wheel family. *J. Am. Chem. Soc.* **2017**, *139*, 18178–18181.

[27] Papatriantafyllopoulou, C.; Moushi, E. E.; Christou, G.; Tasiopoulos, A. J. Filling the gap between the quantum and classical worlds of nanoscale magnetism: Giant molecular aggregates based on paramagnetic 3d metal ions. *Chem. Soc. Rev.* **2016**, *45*, 1597–1628.

[28] Zheng, X. Y. ; Kong, X. J. ; Long, L. S. Synthesis and structures of lanthanide-transition metal clusters. In *Recent Development in*

Clusters of Rare Earths and Actinides: *Chemistry and Materials*; Zheng, Z. P., Ed.; Springer: Berlin Heidelberg, 2017; pp 51–96.

[29] Qin, L.; Zhou, G. J.; Yu, Y. Z.; Nojiri, H.; Schröder, C.; Winpenny, R. E. P.; Zheng, Y. Z. Topological self-assembly of highly symmetric lanthanide clusters: A magnetic study of exchange-coupling "fingerprints" in giant gadolinium(III) cages. *J. Am. Chem. Soc.* **2017**, *139*, 16405–16411.

[30] Crans, D. C.; Ehde, P. M.; Shin, P. K.; Pettersson, L. Structural and kinetic characterization of simple complexes as models for vanadate-protein interactions. *J. Am. Chem. Soc.* **1991**, *113*, 3728–3736.

[31] Graham, K.; Ferguson, A.; Douglas, F. J.; Thomas, L. H.; Murrie, M. Access to an unusual Fe_9 core topology from the initial use of tricine in iron(III) cluster chemistry. *Dalton Trans.* **2011**, *40*, 3125–3127.

[32] Ahmed, I. T. Divalent metal ion ternary complexes of tricine and mercaptobenzazoles. *Synth. React. Inorg. Met. -Org. Chem.* **2003**, *33*, 547–564.

[33] El-Roudi, O. M.; Abd Alla, E. M.; Ibrahim, S. A. Potentiometric studies on the binary complexes of *N*-[tris(hydroxymethyl)methyl]glycine with Th^{4+}, Ce^{3+}, La^{3+}, and UO_2^{2+} and medium effects on a Th-tricine binary complex. *J. Chem. Eng. Data* **1997**, *42*, 609–613.

[34] Gálico, D. A.; Ovens, J. S.; Sigoli, F. A.; Murugesu, M. Room-temperature upconversion in a nanosized $\{Ln_{15}\}$ molecular cluster-aggregate. *ACS Nano* **2021**, *15*, 5580–5585.

[35] Wang, R. Y.; Selby, H. D.; Liu, H.; Carducci, M. D.; Jin, T. Z.; Zheng, Z. P.; Anthis, J. W.; Staples, R. J. Halide-templated assembly of polynuclear lanthanide-hydroxo complexes. *Inorg. Chem.* **2002**, *41*, 278–286.

[36] Huang, W. M.; Zhang, Z. H.; Wu, Y. L.; Chen, W. M.; Rotsch, D. A.; Messerle, L.; Zheng, Z. P. A systematic study of halide-template effects in the assembly of lanthanide hydroxide cluster complexes with histidine. *Inorg. Chem. Front.* **2021**, *8*, 26–34.

[37] Zhou, G. J.; Chen, W. P.; Yu, Y. Z.; Qin, L.; Han, T.; Zheng, Y. Z. Filling the missing links of M_{3n} prototype 3d-4f and 4f cyclic coordination cages: Syntheses, structures, and magnetic properties of the $Ni_{10}Ln_5$ and the Er_{3n} wheels. *Inorg. Chem.* **2017**, *56*, 12821–12829.

[38] Li, Y. L.; Wang, H. L.; Zhu, Z. H.; Li, J.; Zou, H. H.; Liang, F. P. A series of high-nuclear gadolinium cluster aggregates with a magnetocaloric effect constructed through two-component manipulation. *Inorg. Chem.* **2021**, *60*, 16794–16802.

[39] Gaft, M.; Reisfeld, R.; Panczer, G.; Shoval, S.; Champagnon, B.; Boulon, G. Eu^{3+} luminescence in high-symmetry sites of natural apatite. *J. Lumin* **1997**, *72-74*, 572–574.

[40] Xia, Z. G.; Liu, R. S. Tunable blue-green color emission and energy transfer of $Ca_2Al_3O_6F$: Ce^{3+}, Tb^{3+} phosphors for near-uv white LEDs. *J. Phys. Chem. C* **2012**, *116*, 15604–15609.

[41] Yguerabide, J.; Burton, M. Luminescence decay times: Concentration effects. *J. Chem. Phys.* **1962**, *37*, 1757–1774.

Peng-Fei Sun received his bachelor's degree from Northwest Northwest Agriculture & Forestry University in 2020. Currently, he is studying for his Ph.D. degree in Prof. Yan-Zhen Zheng's research group at the Institute of Frontier Science and Technology of Xi'an Jiaotong University. His current research interests is the synthesis of rare earth nanoclusters and their applications in magnetic resonance imaging.

Cai-Hong Fan received her B.S. degree in physics from Shanxi Normal University in 2021. Then, in 2021, she became a graduate student of the Frontier Institute of Science and Technology, Xi'an Jiaotong University, majoring in physics. She is studying for her master's degree under the supervision of Dr. Wei-Peng Chen. Her main research is focused on the preparation and microwave absorption properties of carbon-based composites derived from transition-rare earth metal clusters.

Xiao-Nan Zhang, from Sanmenxia City, Henan Province, entered the School of Hunan University in 2016, majoring in chemistry. Then, in 2020, she became a graduate student of Xi'an Jiaotong University, majoring in chemistry. Currently, she is studying under Prof. Yan-Zhen Zheng. She is mainly engaged in research related to the coordination polymer.

Wei-Peng Chen received his Ph.D. degree in 2017 under the supervision of Prof. Yan-Zhen Zheng. He is currently working at the Institute of Frontier Science and Technology, Xi'an Jiaotong University. His research interests focused on the magnetic refrigeration application of rare earth nanoclusters and CO_2 catalytic performance of rare earth nanoclusters. He has published more than ten papers in well-known academic journals in the field of chemistry. He has presided over the National Natural Science Foundation of China, China Postdoctoral Science Foundation, Shaanxi Provincial Natural Science Foundation Youth Projects, etc. He was selected as the first batch of Xi'an Jiaotong University "Young Outstanding Talents Program" and Shaanxi Provincial Special Support Program "Young Top Talents Program".

Yan-Zhen Zheng was born and raised in Guangdong, China. He received his Ph.D. degree in 2007 under Prof. Xiao-Ming Chen (Sun Yat-Sen University) for studying low-dimensional magnetic coordination polymers. Yan-Zhen then moved to Europe with the supports of Alexander von Humboldt Fellowship under Annie Powell (Karlsruhe Institute of Technology) and Marie Curie International Incoming Fellowship under Richard Winpenny (The University of Manchester) for advanced molecular magnetism study. During this period he had a short postdoctoral training for spintronics under Prof. Paul Kögerler (Forschungszentrum Jülich and RWTH Aachen University). In 2012, he was appointed as a full professor at Xi'an Jiaotong University, where he started his own adventure in molecular magnetism and functional coordination complexes research. In 2014, he was promoted to an associate dean for Frontier Institute of Science and Technology (FIST) and jointly the lab director of Molecular Spin and Electronic Structure (MSES). Currently, the research topics in his group mainly focus on the design and synthesis of single-molecule magnets, functional lanthanide clusters, and electrically-conductive coordination compounds.

https://doi.org/10.26599/POM.2023.9140026
Polyoxometalates, **2023**, *2*, 9140026